Structural Chemistry, Vol. 7, No. 1, 1996

The Vibrational and NMR Spectra, Conformations and ab Initio Calculations of Aminomethylene, Propanedinitrile and Its *N*-Methyl Derivatives

Anton Gatial,[1,6] Štěpán Sklenák,[1,5] Viktor Milata,[2] Peter Klaeboe,[3] Stanislav Biskupič,[1] Dieter Scheller,[4] and Jana Jurašková[1]

Received January 6, 1995; revised April 24, 1995; accepted April 25, 1995

The IR and Raman spectra of aminomethylene propanedinitrile (AM) [$H_2N-CH=C(CN)_2$], (methylamino)methylene propanedinitrile (MAM) [$CH_3NH-CH=C(CN)_2$] and (dimethylamino)methylene propanedinitrile (DMAM) [$(CH_3)_2N-CH=C(CN)_2$] as solids and solutes in various solvents have been recorded in the region 4000–50 cm^{-1}. AM and DMAM can exist only as one conformer. From the vibrational and NMR spectra of MAM in solutions, the existence of two conformers with the methyl group oriented *anti* and *syn* toward the double C=C bond were confirmed. The enthalpy difference $\Delta H°$ between the conformers was measured to be 3.7 ± 1.4 kJ mol^{-1} from the IR spectra in acetonitrile solution and 3.4 ± 1.1 kJ mol^{-1} from the NMR spectra in DMSO solution. Semiempirical (AM1, PM3, MNDO, MINDO3) and ab initio SCF calculations using a DZP basis set were carried out for all three compounds. The calculations support the existence of two conformers *anti* and *syn* for MAM, with *anti* being 7.8 kJ mol^{-1} more stable than *syn* from ab initio and 8.6, 13.4, 11.6, and 10.8 kJ mol^{-1} from AM1, PM3, MNDO, and MINDO3 calculations, respectively. Finally, complete assignments of the vibrational spectra for all three compounds were made with the aid of normal coordinate calculations employing scaled ab initio force constants. The same scale factors were optimized on the experimental frequencies of all three compounds, and a very good agreement between calculated and experimental frequencies was achieved.

KEY WORDS: Vibrational and NMR spectra; conformational analysis; enamines; semiempirical and ab initio calculations.

INTRODUCTION

Enamines are accessible and highly reactive compounds which are very important in a number of synthetic processes [1, 2] and their aminoethylene derivatives of the general formula $R_1R_2N-CR_3=CXY$, where R_1, R_2, and R_3 are H, alkyl or (hetero)aryl, and X and Y are electron-withdrawing groups, are useful as materials for pharmaceutical, dye, perfume, and polymer synthesis. For example *N*-(heteroaryl)-aminoethylene compounds with two electron-withdrawing substituents in β-position are often used in the synthesis with a fused 3-substituted pyridine ring with antibacterial properties [3, 4]. Aminomethylene- and 1-aminoethylidene propanedinitrile and its homologues with the general formula $R_1R_2N-CR_3=C(CN)_2$ represent a group of compounds which also have a wide use in organic synthesis [5]. They are often used as starting reactants or intermediates for the preparation of many compounds, such as vitamin B_1 [6–8] and thiamine [9, 10].

[1] Department of Physical Chemistry, Slovak Technical University, Bratislava, Slovakia.
[2] Department of Organic Chemistry, Slovak Technical University, Bratislava, Slovakia.
[3] Department of Chemistry, University of Oslo, Norway.
[4] Institute of Analytical Chemistry, Technical University Dresden, Dresden, Germany.
[5] Permanent address: Chemical Faculty, Technical University Brno, Veslařská 230, Brno, The Czech Republic.
[6] Correspondence should be directed to Anton Gatial, Department of Physical Chemistry, Slovak Technical University, SK-81237 Bratislava, Slovakia.

1040-0400/96/0200-0017$09.50/0

Despite wide use in organic synthesis, the study of the physical and physicochemical properties of these compounds has been mainly carried out by NMR and UV spectroscopy, where only basic NMR characteristics (chemical shift, coupling constants) and UV maxima were measured [11–16]. Therefore, we decided to study these compounds by vibrational spectroscopy. As a first step we choose the simplest molecules from this group: aminomethylene propanedinitrile and its *N*-methyl derivatives: (R_3=H and R_1 and R_2 are H or CH_3).

Aminomethylene propanedinitrile (AM) [$H_2N-CH=C(CN)_2$], (methylamino)methylene propanedinitrile (MAM) [$CH_3NH-CH=C(CN)_2$], and (dimethylamino)methylene propanedinitrile (DMAM) [$(CH_3)_2N-CH=C(CN)_2$] have not been investigated by vibrational spectroscopy except for a general study in which the C≡N stretching absorptions were determined for 20 compounds of the general formula $R_1R_2C=C(CN)_2$ and correlated with the resonance constants of the R_1 and R_2 substituents [17]. By NMR spectroscopy the barrier to hindered rotation around the C—N amino bond in DMAM was examined [13, 14].

To extend the information about the structure of these molecules, we have also carried out an ab initio study with fully optimized geometries, a determination of the force fields, and a calculation of frequencies for the normal modes of vibrations.

EXPERIMENTAL

Preparative

The compounds have been prepared according to the reaction scheme

$$R_1R_2NH + RO-CH=C(CN)_2 \rightarrow$$

$$R_1R_2N-CH=C(CN)_2 + ROH$$

Ten mmol of ethoxy methylene propanedinitrile was dissolved in a minimum of hot methanol. To the solution was added 12 mmol of the aqueous solution of the corresponding amine. After cooling of the reaction mixture the product was separated and the precipitate was filtered from the reaction mixture, washed with water, dried under vacuum, and purified chromatographically (silicagel, eluent methanol in chloroform 0–50%). When the product did not separate, the reaction mixture was evaporated to dryness and purified chromatographically as in the former case. The purity and melting points were determined by differential scanning calorimetry using a Perkin–Elmer DSC-7 calorimeter. The purity of all three compounds was better than 99%, and the melting points (148°C for AM, 191°C for MAM, and 81°C for DMAM) agree with the literature values [18–20]. The identity and purity of the samples were also confirmed by mass spectroscopy and NMR spectroscopy.

Spectra

Mid-IR spectra in the region 4000–400 cm^{-1} were recorded on Bruker model IFS 88 and on Philips model PU9800 FT-IR spectrometers and the far-IR spectra were recorded on an evacuated Bruker 114c FT-IR spectrometer with 3.5-μm and 12-μm Mylar beam splitters covering the regions 800–100 cm^{-1} and 200–50 cm^{-1}, respectively. The spectra of all the three compounds at room temperature were measured as KBr pellets and as nujol suspensions in the mid-IR region and as PE pellets in the far-IR region. Because the samples are not soluble in CCl_4 or CS_2, we had to use CH_3CN, CH_2Cl_2, and $CHCl_3$ as solvents, and solubility increased in the order AM, MAM, DMAM. IR spectra of the solutions were measured in a cell equipped with KBr windows and a variable path length. The temperature-dependent IR spectra were measured in the region 283–338 K on a heatable cell from Carl-Zeiss with KBr windows and of 0.1-mm path length.

Raman recordings using an argon ion laser were impossible for the three samples due to extremely high fluorescence. Therefore, Bruker RFS 100 and Perkin-Elmer 2000 FT-Raman instruments equipped with an Nd^{3+}:YAG laser were used. Raman spectra at room temperature of powdered solids were obtained for all three samples in the region 4000–50 cm^{-1}. Due to low solubility more than 1000 scans were employed to obtain the Raman spectra for MAM in acetonitrile solution.

The ^{13}C NMR spectra were run at room temperature with a Bruker MSL 300 spectrometer. To obtain frequency resolution of 0.23 Hz/point, zero filling up to 64k was used for gated decoupled spectra before transformation.

RESULTS

A mid-IR survey spectrum of AM as a KBr pellet is shown in Fig. 1, while a Raman spectrum as a solid powder is given in Fig. 2. The wave numbers of the observed IR and Raman bands are listed in Table I.

The corresponding spectra of MAM are shown in Figs. 3 and 4, respectively. The IR and Raman spectra

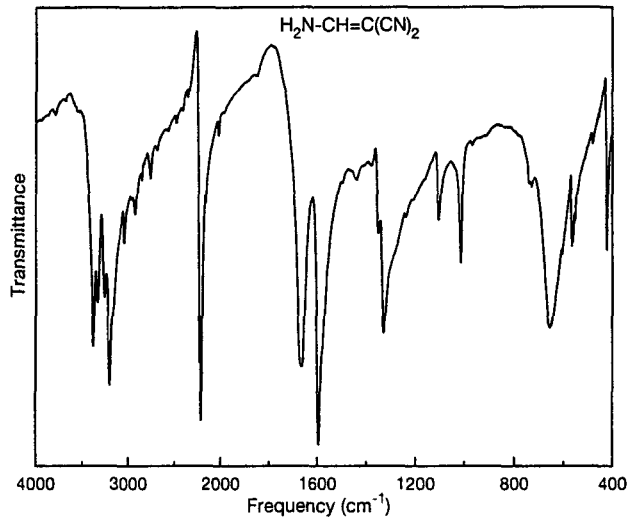

Fig. 1. IR spectrum of AM in KBr pellet at room temperature.

of the solid are compared in Fig. 5 with those of the acetonitrile solution in the region 700–400 cm^{-1}. Some weak Raman bands in acetonitrile solution vanishing in the solid spectra are demonstrated in Fig. 6. IR curves of the acetonitrile solution of MAM between 1730 and 1560 cm^{-1}, shown in Fig. 7, demonstrate the displacement of the conformational equilibrium with temperature. These curves were used for the $\Delta H°$ determination. The experimental wave numbers for MAM are collected in Table II.

A mid-IR spectrum of DMAM as a KBr pellet appears in Fig. 8, whereas a Raman spectrum of a solid powder is given in Fig. 9. The wave numbers of the observed IR and Raman bands are listed in Table III.

A comparison of the ^{13}C NMR spectra of all the three samples in DMSO solution appear in Fig. 10, while the chemical shifts and vicinal coupling constants are listed in Table IV.

Conformational Analysis

The conformational possibility for all three samples is determined by rotation around the C—N bond. Supposedly, the stable configuration of the amino group is that in which the lone electron pair at the amino nitrogen atom is included in a highly conjugated system of the C=C double bond and the triple bonds of both cyano groups. It is obvious that AM and DMAM can

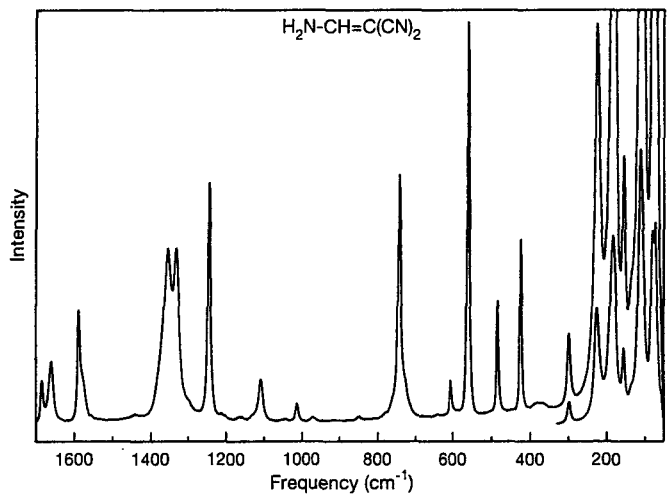

Fig. 2. Raman spectrum of solid AM at room temperature.

Table I. Infrared and Raman Spectral Data[a] for Aminomethylene Propanedinitrile (AM).

Infrared			Raman	
Liquid	Solid		Solid	
CH_3CN[b]	KBr/PE pellet	nujol		Interpretation
3422 s[c]	3381 s	3378 s	3379 vw	ν_1
3356 vs	3338 s	3335 s	3334 vw	
3280 s	3266 s	3264 s	3262 vw	ν_2
3227 s	3209 s	3202 s	3204 w	
	3173 s,sh	3173 s,sh		$2\nu_7 = 3188$
3055 w	3044 m	3044 m	3044 w	ν_3
	2920 vw			
	2350 vw	2352 vw		
2220 vs	2227 s	2228 s	2223 vs	ν_4
2210 vs	2209 vs	2209 vs	2210 vs	ν_5
2163 w	2168 w,sh	2168 w,sh	2167 vw	
	2159 w,sh	2159 w,sh	2158 w	
	2020 w	2020 w	2020 vw	$2\nu_{18} = 2028$
	1989 vw			$\nu_9 + \nu_{19} = 1984$
	1852 vw			
			1684 vw	
1662 vs	1665 vs	1670 vs	1659 w	ν_6
1591 vs	1594 vs	1594 vs	1588 m	ν_7
	1577 s,h	1577 s,sh	1579 w,sh	$\nu_{18} + \nu_{20} = 1581$
	1500 vw	1499 vw		$\nu_{18} + \nu_{21} = 1495$
	1442 vw			$2\nu_{12} = 1458$
	1383 vw			$\nu_{12} + \nu_{19} = 1383$
1350 m,sh	1350 m	1350 m	1354 s	ν_8
1329 s	1330 s	1329 s	1332 s	ν_9
	1303 m,sh	1300 m,sh		$2\nu_{19} = 1308$
1234 w	1240 w	1240 w	1244 s	ν_{10}
	1209 vw	1210 vw	1210 vw	$\nu_{19} + \nu_{20} = 1221$
1155 vw	1171 vw	1170 vw	1170 vvw	$\nu_{13} + \nu_{20} = 1172$
1099 m	1105 m	1105 m	1108 w	ν_{11}
1002 m	1014 m	1015 m	1013 w	ν_{18}
959 vw	968 vw	968 vw	968 vw	$\nu_{14} + \nu_{15} = 976$
	845 vw	845 vw		$2\nu_{15} = 846$
	818 vw			$\nu_{16} + \nu_{19} = 825$
	783 vw	783 vw,sh		$\nu_{21} + \nu_{22} = 780$
	740 w,sh	739 w	740 s	
732 w	729 m	725 ?	730 w,sh	ν_{12}
623 s	654 vs	654 vs		ν_{19}
	605 m,sh	609 m,sh	605 w	ν_{13}
567 m	567 s	567 m		ν_{20}
	562 s,sh		558 s	
552 m,sh	553 m,sh	554 m,sh	553 w,sh	ν_{14}
475 w	481 w	482 w	484 w	ν_{21}
416 m	423 s	423 s	424 m	ν_{15}
	299 w	298 w	298 m	ν_{22}
	203 m,sh		224 s	ν_{23}
	196 s,sh			
	185 s,sh		184 s	ν_{24}
	171 s			
			155 m	ν_{16}
	138 w		136 w	
	108 s		111 s	ν_{17}
	102 s,sh			

Table I. Continued.

Infrared			Raman	
Liquid	Solid		Solid	
CH_3CN^b	KBr/PE pellet	nujol		Interpretation
			81 s	
			73 s	
	56 m		58 w	

[a] Weak bands in the regions 4000–3500 and 2900–2400 cm^{-1} have been omitted.
[b] Solvent used.
[c] Abbreviations: s, strong; m, medium; w, weak; v, very; sh, shoulder.

exist as only one conformer independent of the structure of the amino group (pyramidal or planar). It means that only MAM can exist in two conformations with the methyl group oriented out from the C=C double-bond *anti* conformer and toward the C=C double-bond *syn* conformer:

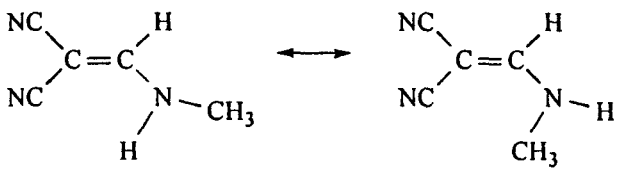

anti *syn*

We might intuitively assume from steric reasons that *anti* will be the more stable conformer, suppored by ab initio calculations and from the vibrational spectra.

Like all compounds with a cyano group these samples also have very small vapor pressue and low solu-

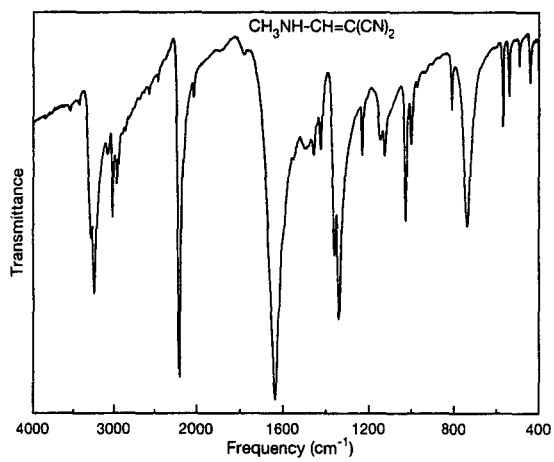

Fig. 3. IR spectrum of MAM in KBr pellet at room temperature.

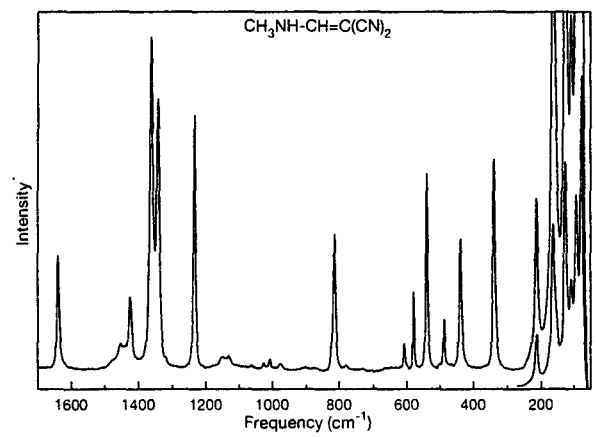

Fig. 4. Raman spectrum of solid MAM at room temperature.

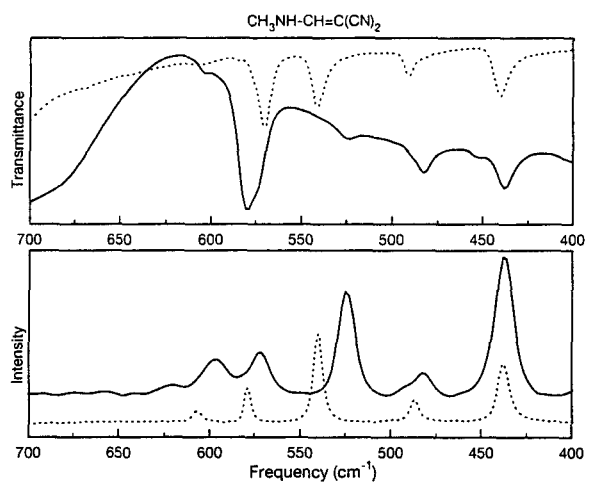

Fig. 5. IR spectra (top) of MAM in KBr pellet (dashed line) and as solution in acetonitrile (solid line) and Raman spectra (bottom) of solid MAM (dashed line) and as a solute in acetonitrile (solid line) at room temperature.

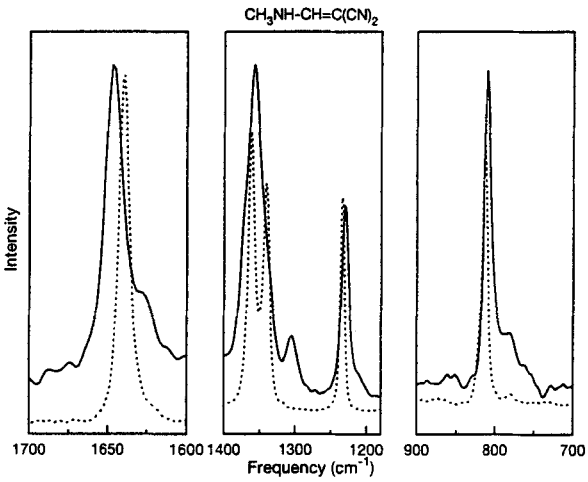

Fig. 6. Raman spectra of solid MAM (dashed line) and as a solution in acetonitrile (solid line) at room temperature.

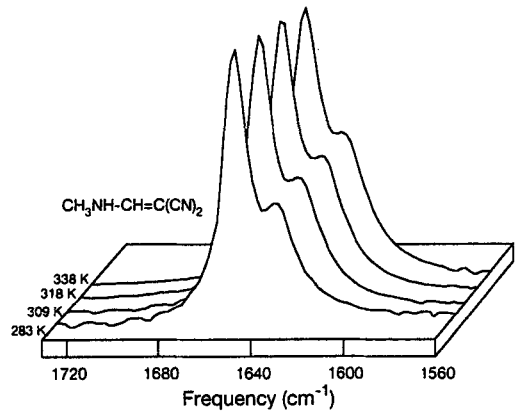

Fig. 7. IR temperature-dependent spectra of MAM in acetonitrile solution.

bility in most solvents. AM is soluble only in a very polar solvents (CH_3CN) in a small amount, and only the strongest bands in the IR solution spectra could be obtained. On the opposite side the best soluble sample is DMAM, and for this sample also IR spectra in a less polar solvent (CH_2Cl_2 and $CHCl_3$) could be obtained. In the solution spectra of these two compounds we did not find bands missing in solid-phase spectra.

Relatively good IR spectra in acetonitrile solution with different path length could be obtained for MAM, but only weak solution spectra in less polar solvents (CH_2Cl_2 and $CHCl_3$) due to very low solubility were measured. From a comparison of the IR spectra in solution and in the solid phase, we have found some bands which disappear in the latter spectra. These bands are present in acetonitrile solution at 1630, 1370, 780, 689, 570, 490, and 452 cm^{-1}. An attempt was made to confirm this conclusion, and several Raman spectra of

Table II. Infrared and Raman Spectral Data[a] for (Methylamino)methylene Propanedinitrile (MAM).

Infrared			Raman		
Liquid	Solid		Liquid		Interpretation
CH_3CN[b]	KBr/PE pellet	Nujol	CH_3CN[b]	Solid	*anti* *syn*
3330 s[c]	3287 s	3283 s	3326 vvw	3280 vw	ν_1
3270 m	3250 s	3249 s	3275 vvw	3245 w	
3090 w	3085 w	3075 w	3084 ?	3070 vw	ν_2
3081 vw,sh	3076 vw,sh		3074 w		
3036 w	3024 m	3021 m	3038 w	3024 w	ν_3
2974 vw	2969 m		2978 w	2965 w,sh	ν_{23}
	2949 w			2948 mw	ν_4
	2906 vw				$2\nu_9 = 2916$
2860 vw	2864 vw		2856 vw	2864 vw	$\nu_{10} + \nu_{24} = 2869$
2232 vw,sh	2238 w,sh	2236 w,sh			
2215 vs	2218 vs	2217 vs	2215 vs	2215 vs	ν_5
2205 vs	2203 vs	2203 vs	2208 s,sh	2202 vs	ν_6
2161 vw	2161 w	2163 w			
	2042 w	2041 w		2042 vw	$2\nu_{26} = 2054$
	1895 vw				$\nu_{11} + \nu_{18} = 1901$
	1782 w				$\nu_{12} + \nu_{19} = 1779$

Table II. Continued.

Infrared			Raman			
Liquid	Solid		Liquid		Interpretation	
CH_3CN^b	KBr/PE pellet	Nujol	CH_3CN^b	Solid	*anti*	*syn*
1648 vs	1637 vs	1636 vs	1647 w	1639 m	ν_7	
1630 s	*	*	1629 vw,sh	*		ν_7
1553 w	1552 w	1561 w	1548 vvw	*	$\nu_{16} + \nu_{27} = 1553$	ν_8?
	1500 vw	1507 vw,sh			$\nu_{15} + \nu_{29} = 1493$	
1485 vw	1482 vw	1497 vw,sh	1482 vw		ν_8	
1460 vw	1458 w		1459 vw,sh	1451 vw	ν_9	
1443 w	1443 vw,sh		1447 w	1441 vw	ν_{24}	
1426 m	1426 m	1433 m	1424 m	1424 mw	ν_{10}	
1370 m,sh	*	*	1369 m,sh	*		ν_{11}?
1360 m	1360 s	1364 s	1358 s	1362 s	ν_{11}	
1337 s	1339 s	1341 s	1343 s,sh	1342 s	ν_{12}	
			1305 w	*		ν_{12}
1231 w	1234 m	1233 m	1230 m	1235 s	ν_{13}	
			1209 vw,sh	*		ν_{13}?
1136 m	1148 m	1150 m	1142 vw	1150 vw	ν_{25}	
1123 w	1129 m	1129 m	1125 vvw	1130 vw	ν_{14}	
	1098 w,sh	1098 w,sh			$\nu_{18} + \nu_{28} = 1111$	
	1078 w,sh				$2\nu_{18} = 1082$	
1003 m,sh	1027 s	1026 s	1025 vw	1027 vvw	ν_{26}	
992 m	1002 m	1001 m	1005 vw	1008 vw	ν_{15}	
974 w,sh	975 w	974 w	968 vw	974 vw	$2\nu_{29} = 982$	
	942 vw	939 vw			$\nu_{19} + \nu_{29} = 931$	
	909 vw				$\nu_{20} + \nu_{28} = 908$	
808 w	813 m	812 m	810 w	813 m	ν_{16}	
780 ?	*	*	782 vw,sh	*		ν_{16}
710 m	740 s	736 s			ν_{27}	
	710 m,sh					
689 m,sh	*	*				ν_{27}
602 vw	606 vw	606 vw	620 vw	607 w	ν_{17}	
579 s	570 s	569 s	596 w	579 mw	ν_{28}	
570 m,sh	*	*	571 w	*		ν_{28}
526 w	541 s	540 m	525 m	540 s	ν_{18}	
490 vw,sh	*	*	490 w	*		ν_{29}
482 w	491 m	490 w	482 w	486 mw	ν_{29}	
452 vw	*	*				ν_{19}
436 w	440 m	440 m	437 m	437 s	ν_{19}	
	436 w,sh					
320 ?	338 m	338 m	332 w	339 s	ν_{20}	
	330 w	332 w	321 vw,sh	333 w,sh	ν_{30}	
			263 vw	*		ν_{30}?
	226 m	226 m	194 m,sh	213 mw	ν_{31}	
	170 s					
	161 m,sh		149 vs	163 s	ν_{21}	
				154 w,sh		
	123 m		128 vs	126 s	ν_{32}	
	107 s			108 w	ν_{22}	
				92 s		
	76 m			77 s	ν_{33}	

[a] Weak bands in the regions 4000–3400 and 2800–2300 cm^{-1} have been omitted.

[b] Solvent used.

[c] Abbreviations: s, strong; m, medium; w, weak; v, very; sh, shoulder; * denotes bands vanishing in the solid phase.

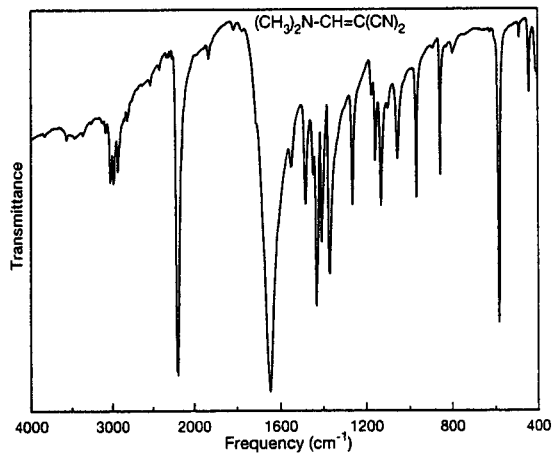

Fig. 8. IR spectrum of DMAM in KBr pellet at room temperature.

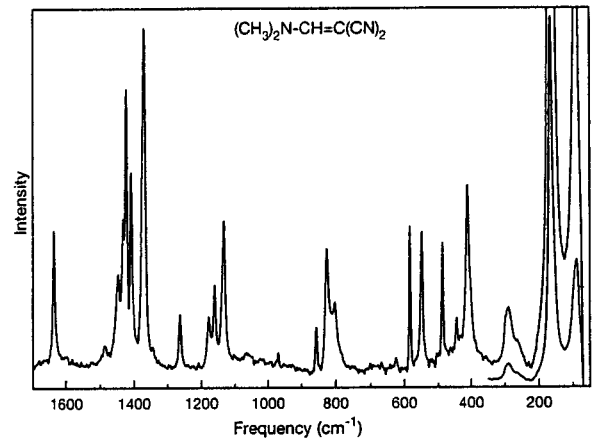

Fig. 9. Raman spectrum of a solid DMAM at room temperature.

MAM in acetonitrile solution were recorded. Unfortunately, in an almost saturated solution and up to 4000 scans the weak Raman bands are only slightly above the noise level. Despite this, a comparison of the Raman solid and acetonitrile solution spectra is possible, as can be seen in Fig. 6, and the result from IR spectra can be confirmed also from the Raman spectra. Furthermore, some additional disappearing bands at 1548, 1305, and 263 cm^{-1} have been detected. These facts support the conclusion that MAM exists in two conformational forms in acetonitrile solution.

These results were also confirmed by NMR spectroscopy. The ^{13}C and ^{1}H NMR spectra of AM, MAM, and DMAM in DMSO have been measured at room temperature (Fig. 10). In these spectra each main band has a weaker counterpart only in the spectrum of MAM, meaning that the room temperature is below the coalescence temperatures and confirms the existence of two

Table III. Infrared and Raman Spectral Data[a] for (Dimethylamino)methylene Propanedinitrile (DMAM).

Infrared				Raman	
Liquid		Solid		Solid	
CH_2Cl_2[b]	CH_3CN[b]	KBr/PE pellet	Nujol		Interpretation
		3080 vw[c]	3074 vw	3079 vw	ν_1
3030 w		3025 w	3023 w	3027 w,sh	ν_2, ν_3
		3009 vw	3013 vw	3011 m	ν_4
2980 w		2987 w		2979 m	ν_5
		2984 w,sh			
2930 m		2933 w		2937 s	ν_6
		2924 vw,sh			ν_7
		2884 vw,sh			$\nu_{11} + \nu_{17} = 2892$
		2852 vw			$2\nu_{14} = 2866$
		2833 vw			$\nu_{16} + \nu_{17} = 2836$
		2814 vw,sh	2815 vw,sh	2815 w	$2\nu_{17} = 2818$
		2289 vw	2290 vw		
2261 vw		2260 vw	2261 vw		
2217 vs	2219 vs	2213 vs	2217 s,sh	2209 vs	ν_8
2205 vs	2207 vs	2199 vs	2199 vs	2200 vs	ν_9
2155 vw	2155 vw	2154 m,sh	2155 m,sh		
		2144 m,sh	2145 m,sh		
		2136 w,sh	2136 w,sh		

Table III. Continued.

Infrared				Raman	
Liquid		Solid		Solid	
CH_2Cl_2[b]	CH_3CN[b]	KBr/PE pellet	Nujol		Interpretation
1900 vw	1891 vw	1930 w	1929 w	1926 w	$2\nu_{25} = 1938$
		1813 vw	1815 vw		$\nu_{17} + \nu_{33} = 1818$
		1774 vw	1777 vw		$\nu_{18} + \nu_{33} = 1780$
		1711 w,sh	1710 w,sh		$2\nu_{26} = 1714$
1638 vs	1644 vs	1646 vs	1648 vs	1638 m	ν_{10}
		1614 w,sh	1611 w,sh		
1544 w		1550 w	1549 w		$\nu_{25} + \nu_{29} = 1552$
1482 m		1483 s	1484 s	1486 vw	ν_{11}, ν_{12}
		1448 m	1450?	1447 w	ν_{13}
1436 s		1433 s	1434 s	1433 m,sh	ν_{14}, ν_{15}
1424 s		1427 m,sh	1428 m,sh	1424 s	ν_{16}
1408 s		1409 s	1410 m	1409 m	ν_{17}
		1402 m,sh	1404 w,sh		
1368 s	1368 s	1371 s	1370?	1370 s	ν_{18}
1333 vw,sh		1341 w,sh	1342 w,sh	1344 vw	
		1310 vw	1300 vw		$\nu_{26} + \nu_{32} = 1300$
	1264 w	1263 s	1260 s	1264 m	ν_{19}
1172 vw	1176 vw	1175 w	1175 w	1178 w	ν_{20}
1154 w	1157 w	1158 m	1158 m	1160 mw	ν_{21}
1129 s	1132 s	1131 m	1132 m	1134 m	ν_{22}
	1100 vw,sh	1099 w	1100 w	1107 wv	ν_{23}
1059 m		1055 m	1055 m	1075 vw	ν_{24}
		1024 vw,sh	1021 vw,sh		$\nu_{29} + \nu_{32} = 1026$
954 m	957 m	969 s	968 s	972 vw	ν_{25}
		890 vw	891 vw		$2\nu_{32} = 886$
859 m	857 w	857 s	857 s	857 w	ν_{26}
817 w	819 vw	830 vw	828 vw	825 m	ν_{27}
		797 w	799 w	802 w	$2\nu_{34} = 806$
625 vw		624 vw	625 vw	626 vw	ν_{28}
602 vw		599 vw,sh	600 vw,sh		
585 s	585 s	583 vs	585 vs	584 m	ν_{29}
				548 m	ν_{30}
498 vw		498 w	498 w	487 m	ν_{31}
		487 vw			
444 w		443 m	444 m	444 vw	ν_{32}
400 vw,sh		409 m	409 m	411 m	ν_{33}
391 w		403 m	403 m	405 w,sh	ν_{34}
		367 vw	365 vw		
		289 w,sh	286 w	287 mw	ν_{35}
		261 m	259 m	258 vw	ν_{36}
		196 w			ν_{37}
		176 m,sh			ν_{38}
		168 m		164 vs	ν_{39}
		158 m,sh			ν_{40}
		100 m,sh			
		92 m		89 s	ν_{41}
		84 m			
		64 m			
		58 m		58 w,sh	ν_{42}

[a] Weak bands in the regions 4000–3100 and 2800–2300 cm^{-1} have been omitted.
[b] Solvents used.
[c] Abbreviations: s, strong; m, medium; w, weak; v, very; sh, shoulder.

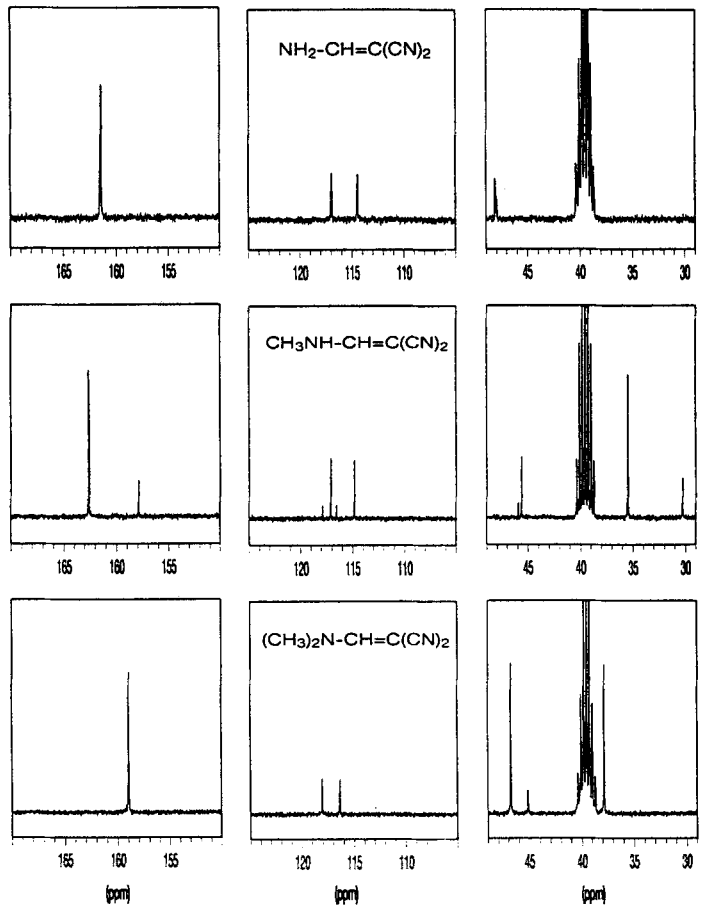

Fig. 10. NMR spectra of AM, MAM, and DMAM in DMSO solution at room temperature.

Table IV. ^{13}C NMR Data of the Compounds $R_1R_2N-CH=(CN)_2$.

Compound	AM $R_1=R_2=H$	MAM-*anti* $R_1=CH_3$, $R_2=H$	MAM-*syn* $R_1=H$, $R_2=CH_3$	DMAM $R_1=R_2=CH_3$
Chemical shifts[a] in ppm				
C_1	48.1	45.6	45.9	45.1
C_2	161.4	162.1	157.9	158.9
C_7	116.9	117.1	117.8	118.0
C_9	114.4	114.8	116.5	116.3
C_4		35.4		46.8
C_6			30.1	37.8
Vicinal coupling constants[a] in Hz				
H_5-C_7	4.6	4.6	5.5	5.5
H_5-C_9	10.4	10.2	11.1	10.6
H_5-C_4		5.3		5.1
H_5-C_6			7.9	6.5
H_4-C_1	2.0		1.2	

[a] Numbering of the atoms according to Fig. 11.

conformers for this sample. More detailed NMR temperature studies in different solvents together with DNMR investigations of the barrier of the hindered rotation in the amino group will appear in a separate article [21].

Conformational Energy Difference

The enthalpy difference between the two conformers of MAM in solution can be determined from temperature studies of the appropriate IR spectra. The best band pairs should be conformationally pure belonging to the *anti* and *syn* conformer with sufficient intensity and separation. From all the MAM bands in acetonitrile solution mentioned above, only one band is useful: 1630 cm^{-1} for the *syn* conformer and 1648 cm^{-1} for the *anti* conformer. Thus, in the variable-temperature cell the solution spectra were recorded in the temperature range 283–338 K. A band separation procedure was employed since the 1630- and 1648-cm^{-1} bands overlapped slightly and band areas were used for determining the equilibrium constant K at different temperatures.

By applying the van't Hoff equation we have determined $\Delta H°$ by making a plot of ln K versus 1/T, where $\Delta H°/R$ is the slope of the line obtained by a least-squares procedure. It is assumed that $\Delta H°$ is not a function of temperature in such a short interval. A value $\Delta H°$(*syn–anti*) = 3.7 ± 1.4 kJ mol^{-1} has been obtained.

A similar value was obtained from the ^1H NMR spectra where bands corresponding to the —CH=proton for both conformers were measured in the temperature range 295–353 K. Using band areas for determining the equilibrium constant K at different temperatures and using the same procedure, we have obtained $\Delta H°$ = 3.4 ± 1.1 kJ mol^{-1}.

Semiempirical and ab Initio Calculations

Since there are no reported experimental data regarding the structure, conformational energies, and vibrational assignments of the present molecules, we carried out semiempirical and ab initio calculations to support the interpretations. The semiempirical (AM1, PM3, MNDO, and MINDO3) methods were employed using the MOPAC program [22]. For the ab initio Hartree–Fock SCF calculations the HONDO-like program and the standard Huzinaga DZP basis set [23, 24] were employed. To improve the accuracy of the ab initio energies, MP2 corrections were carried out but geometries of the molecules were not reoptimized at the MP2/SCF level.

A decreasing character of the pyramidal structure of the amino group from CH_3NH_2 to $CH_2{=}CHNH_2$ has been measured [25, 26]. A nearly planar structure of the amino group is expected in the present molecules due to the strongly electron withdrawing cyano groups. Similarly in substituted aniline a planar structure was calculated [27] due to electron-withdrawing groups in the benzene ring. Thus, the crucial point for interpreting the vibrational spectra of the present molecules is whether the moiety of the amino group $=CH-NR_1R_2$ is planar or nonplanar. If it is planar does the plane of the amino group orient in the plane of the rest of molecule? In the latter case the molecule may have C_s symmetry, while otherwise the molecule lacks symmetry. In all the semiempirical and ab initio calculations the full set of structural parameters were optimized with no assumptions regarding symmetry. The results of the torsional angles for the $C{=}CH-NR_1R_2$ moiety (R_1 and R_2 is H or C) are found in Table V.

From these results it is obvious that ab initio, AM1, and MINDO3 methods give nearly planar structures of the amino group for AM and for both conformers of MAM with a small exception for the *anti* conformer of MAM in the AM1 method. In this case the energy is only 0.07 kJ mol^{-1} higher for the fixed planar structure. PM3 and MNDO give for these molecules only nonplanar pyramidal structures of the amino group. If the plane of symmetry was fixed, the obtained energies were significantly higher and the vibrational analysis gave one negative vibrational mode, meaning that a planar structure can be a saddle point for inversion processes.

In DMAM a nearly planar structure was suggested only when the AM1 method is employed. The other semiempirical methods give nonplanar structures with different geometry of the amino group. While the PM3 method gives the pyramidal structure of the amino group, the MNDO and MINDO3 methods reveal planar structure of the $C-NC_2$ moiety but turn 10–20 degrees from the plane of rest of molecule. The ab initio suggests a slightly nonplanar structure for this molecule probably due to steric interactions of both methyl groups.

As the most acceptable results we consider the ab initio calculations which were calculated with a relatively large basis set. Refinement of the ab initio geometry was carried out until the norm of gradient was lower than 10^{-4} a.u. (most of them in the range 10^{-5}) and the vibrational analysis gave only nonnegative vibrational modes. The obtained internal coordinates with their names and labeling according to Fig. 11 are listed in Table VI. Since we do not have experimental struc-

Table V. Torsional Angles[a] of the Amino Group for the AM, MAM, and DMAM Calculated by ab Initio and Semiempirical Methods.

Sample	Method	$t(C_1{=}C_2{-}N_3{-}X_4)$[b]	$t(C_1{=}C_2{-}N_3{-}X_6)$	$t(H_5{-}C_2{-}N_3{-}X_4)$
AM	ab initio	180.91	−0.65	1.08
	AM1	180.00	0.00	0.00
	PM3	154.92	20.78	−30.55
	MNDO	157.06	24.78	−28.12
	MINDO3	180.02	−0.06	0.04
anti MAM	ab initio	180.02	0.02	0.03
	AM1	174.46	3.80	−6.74
	PM3	159.77	20.80	−25.13
	MNDO	167.21	10.63	−15.57
	MINDO3	179.99	0.02	−0.01
syn MAM	ab initio	179.94	0.10	0.09
	AM1	180.00	0.00	0.00
	PM3	158.75	20.01	−26.87
	MNDO	179.00	1.92	−2.03
	MINDO3	179.92	−0.02	−0.07
DMAM	ab initio	183.86	0.71	4.02
	AM1	179.58	0.29	−0.52
	PM3	163.33	18.46	−21.75
	MNDO	167.43	−18.31	−11.44
	MINDO3	169.97	−10.08	−9.47

[a] Torsional angles in degrees.
[b] Numbering of the atoms according to Fig. 11.

tural data for any of these molecules, the reliability of the ab initio structures is difficult to ascertain. Nevertheless, for interpreting the vibrational spectra we have accepted planar structures with C_s symmetry for AM and MAM and a nonplanar structure with C_1 symmetry for DMAM.

In all five methods the *anti* conformer was the more stable conformer for MAM. From the ab initio calculations in a DZP basis set at SCF level the *anti* conformer is 11.1 kJ mol^{-1} more stable. After including the MP2 corrections and zero-point vibrational energy, the *anti* conformer is 7.8 kJ mol^{-1} at the MP2/SCF level and 8.5 kJ mol^{-1} at the VIB0/MP2/SCF level more stable. For AM1, PM3, MNDO, and MINDO3 the values 8.6, 13.4, 11.6, and 10.8 kJ mol^{-1} have been calculated.

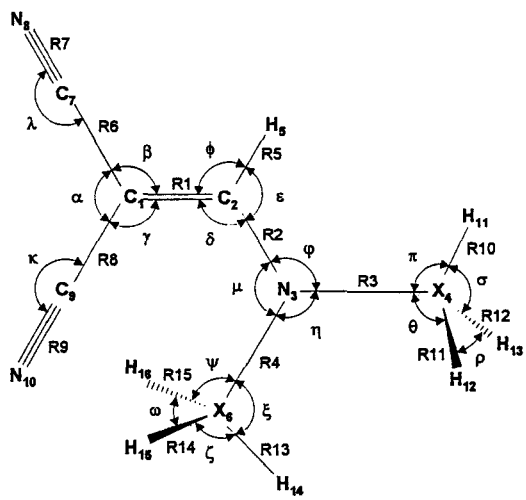

Fig. 11. Internal coordinates for AM (X_4 = X_6 = H), *anti* MAM (X_4 = C, X_6 = H), *syn* MAM (X_4 = H, X_6 = C), and DMAM (X_4 = X_6 = C).

Normal Coordinate Analysis

In order to obtain a more complete description of the molecular motions involved in the normal vibration of all the three samples studied, we have carried out a normal coordinate analysis. The ab initio force fields in Cartesian coordinates calculated in a DZP basis set at the SCF level were transformed to suitable internal coordinates.

It is well known that the ab initio SCF results in different basis sets systematically overestimate the (harmonic) force field by 10–20% but after a suitable correction give an accurate prediction of the vibrational fundamentals [28]. Therefore the ab initio force fields in internal coordinates for all three samples were subsequently scaled according to the type of internal coordinates, using the scheme F_{ij}(scaled) = F_{ij}(ab initio)(x_i

Table VI. Ab Initio Structural Parameters[a] for AM, MAM, and DMAM.

Name[b]	Internal coordinate[c]	AM	MAM		DMAM
			anti	*syn*	
R1	$r(C_1{=}C_2)$	1.3570	1.3622	1.3618	1.3677
R2	$r(C_2{-}N_3)$	1.3273	1.3226	1.3259	1.3242
R3	$r(N_3{-}H_4)$	0.9954		0.9961	
R3	$r(N_3{-}C_4)$		1.4460		1.4521
R4	$r(N_3{-}H_6)$	0.9995	1.0013		
R4	$r(N_3{-}C_6)$			1.4517	1.4552
R5	$r(C_2{-}H_5)$	1.0808	1.0815	1.0811	1.0803
R6	$r(C_1{-}C_7)$	1.4309	1.4298	1.4347	1.4341
R7	$r(C_7{\equiv}N_8)$	1.1343	1.1347	1.1345	1.1348
R8	$r(C_1{-}C_9)$	1.4320	1.4305	1.4334	1.4326
R9	$r(C_9{\equiv}N_{10})$	1.1347	1.1351	1.1343	1.1346
R10	$r(C_4{-}H_{11})$		1.0863		1.0853
R11	$r(C_4{-}H_{12})$		1.0885		1.0899
R12	$r(C_4{-}H_{13})$		1.0885		1.0891
R13	$r(C_6{-}H_{14})$			1.0855	1.0883
R14	$r(C_6{-}H_{15})$			1.0869	1.0851
R15	$r(C_6{-}H_{16})$			1.0869	1.0856
δ	$\angle(C_1{=}C_2{-}N_3)$	126.38	126.54	130.95	131.68
ϕ	$\angle(C_1{=}C_2{-}H_5)$	118.08	117.71	115.45	114.38
φ	$\angle(C_2{-}N_3{-}H_4)$	120.71		115.49	
φ	$\angle(C_2{-}N_3{-}C_4)$		124.86		119.96
μ	$\angle(C_2{-}N_3{-}H_6)$	121.33	117.58		
μ	$\angle(C_2{-}N_3{-}C_6)$			127.73	123.39
β	$\angle(C_2{=}C_1{-}C_7)$	120.02	119.84	117.64	117.02
χ	$\angle(C_2{=}C_1{-}C_9)$	120.15	120.26	125.31	126.44
λ	$\angle(C_1{-}C_7{=}N_8)$	179.00	178.91	178.90	178.94
κ	$\angle(C_1{-}C_9{\equiv}N_{10})$	176.36	176.28	179.38	178.74
π	$\angle(N_3{-}C_4{-}H_{11})$		109.40		110.12
θ_1	$\angle(N_3{-}C_4{-}H_{12})$		110.78		110.63
θ_2	$\angle(N_3{-}C_4{-}H_{13})$		110.79		110.40
ξ	$\angle(N_3{-}C_6{-}H_{14})$			107.62	108.18
ψ_1	$\angle(N_3{-}C_6{-}H_{15})$			111.37	111.51
ψ_2	$\angle(N_3{-}C_6{-}H_{16})$			111.38	111.01
$t1$	$t(C_1{=}C_2{-}N_3{-}H_4)$	180.91		179.84	
$t1$	$t(C_1{=}C_2{-}N_3{-}C_4)$		180.02		183.86
$t2$	$t(C_1{=}C_2{-}N_3{-}H_6)$	−0.65	0.02		
$t2$	$t(C_1{=}C_2{-}N_3{-}C_6)$			0.10	0.71
$t3$	$t(H_5{-}C_2{-}N_3{-}H_4)$	1.08		0.09	
$t3$	$t(H_5{-}C_2{-}N_3{-}C_4)$		0.03		4.02
$t4$	$t(N_3{-}C_2{=}C_1{-}C_7)$	180.22	180.00	180.01	181.14
$t5$	$t(N_3{-}C_2{=}C_1{-}C_9)$	0.23	0.00	−0.04	1.89
$t6$	$t(C_2{-}N_3{-}C_4{-}H_{11})$		0.14		−3.33
$t7$	$t(C_2{-}N_3{-}C_4{-}H_{12})$		119.65		116.53
$t8$	$t(C_2{-}N_3{-}C_4{-}H_{13})$		240.61		236.84
$t9$	$t(C_2{-}N_3{-}C_6{-}H_{14})$			180.13	172.50
$t10$	$t(C_2{-}N_3{-}C_6{-}H_{15})$			−60.77	−68.00
$t11$	$t(C_2{-}N_3{-}C_6{-}H_{16})$			61.02	53.62
$l1$[d]	$l(C_2C_7C_1N_8)$	0.14	0.02	−0.25	0.32
$l2$[d]	$l(C_2C_9C_1N_{10})$	−0.11	0.00	0.33	−2.87

[a] Bond lengths in Angstroms, bond and torsion angles in degrees.
[b] Internal coordinate symbol.
[c] Numbering of the atoms according to Fig. 11.
[d] Coordinate describing linear part of molecule in degrees.

$\cdot x_j)^{1/2}$, where x_i and x_j are scaling factors for the diagonal constants [29]. Initially, all the scaling factors were kept fixed at a value of 1.0 to produce the pure ab initio calculated vibrational frequencies. These vibrational frequencies were found to be 8% to 18% higher than the experimental ones for all three samples. Subsequently, in the first scaling step we have used the scaling scheme preferred by Durig *et al.* [28], and scaling factors of 0.9 for the stretching, 0.8 for the bending and 1.0 for the out-of-plane and torsional coordinates were used. After this scaling procedure the agreement with experimental frequencies was improved to 4–6%, but there are still well-localized vibrational modes like N—H and C≡N stretching and =C—H wagging, which are overestimed up to 12%.

In the second step we choose for such vibrational modes separate scaling factors. This means that we added the separate scaling factors for each of the N—H, C—H, and C≡N stretching coordinates and one common scaling factor for the hydrogen wagging coordinates (for =C—H, $-NH_2$, and —N—H wagging coordinates). We have also included a separate scaling factor for C—C≡N linear bending [30, 31]. All eight scaling factors were then optimized on the 85 experimental frequencies of all the three samples. We obtained the final scaling factors: 0.851 for stretching, 0.827 for bending, 0.874 for torsion and out of plane, 0.754 for N—H stretching, 0.837 for C—H stretching, 0.720 for C≡N stretching, 0.750 for hydrogen wagging, and 0.770 for C—C≡N linear bending coordinates. Frequencies calculated with these scaling factors and the corresponding potential energy distributions (PED) for all three samples are given in Tables VII–X. Agreement with experimental frequencies was improved to 3% outside the low-frequency region below 250 cm^{-1} where data from the fluid phases are missing and the assignment is also rather uncertain due to lattice modes.

DISCUSSION

Geometry

Experimental structure data are not available for the molecules studied, and therefore the reliability of the calculated geometrical values can be tested only in comparison with similar compounds.

Table VII. Comparison of Observed and Calculated Vibrational Frequencies for AM.

No.	Fundamental[a]	Obs.[b]	ab Initio	Scaled[c]	PED[d]
ν_1 A'	NH_2 asym stretch	3422	3943	3423	95 NH_2 as
ν_2	NH_2 sym stretch	3280	3800	3300	96 NH_2 ss
ν_3	=C—H stretch	3055	3375	3088	99 CH s
ν_4	C≡N stretch	2220	2593	2220	87 C≡N s
ν_5	C≡N stretch	2210	2585	2213	88 C≡N s
ν_6	C=C stretch	1662	1821	1666	31 C=C s, 36 NH_2 δ, C—N s
ν_7	NH_2 deformation	1591	1745	1593	59 NH_2 δ, 30 C=C s
ν_8	=C—H rock	1350	1482	1354	30 C—H ro, 19 C=C s, 13 C—N s
ν_9	=C—N stretch	1329	1422	1300	36 C—N s, 29 C—H ro, 13 NH_2 ro
ν_{10}	CC_2 asym stretch	1234	1338	1223	44 CC_2 as, 16 C—N s
ν_{11}	NH_2 rock	1099	1180	1074	60 NH_2 ro, 18 CC_2 as, 15 C—H ro
ν_{12}	CC_2 sym stretch	732	798	727	34 CC_2 ss, 11 C=C s, 11 CC_2 δ
ν_{13}	CC_2 deformation	605	659	593	25 CC_2 δ, 26 CC≡N sδ, 26 CC_2 ss
ν_{14}	C—C≡N asym bend	552	605	547	16 CC≡N aδ, 22 CC_2 ro, 12 C=CN δ
ν_{15}	C=C—N bend	416	462	413	43 C=CN δ, 47 CC≡N aδ
ν_{16}	CC_2 rock	171	182	164	50 CC_2 ro, 31 CC≡N aδ, 13 C=CN δ
ν_{17}	C—C≡N sym bend	111	150	134	57 CC≡N sδ, 50 CC_2 δ
ν_{18} A''	=C—H wag	1002	1125	993	78 C—H wa
ν_{19}	NH_2 torsion	623	733	667	25 NH_2 τ, 29 CC≡N sδ, 29 CC_2 wa
ν_{20}	C—C≡N sym bend	567	613	554	30 CC≡N sδ, 6 CC_2 wa, 33 NH_2 τ
ν_{21}	C—C≡N asym bend	475	537	478	75 CC≡N aδ, 8 C=C τ, 10 NH_2 τ
ν_{22}	NH_2 wag	298	334	295	47 NH_2 wa, 15 C=C τ, 13 CC≡N aδ
ν_{23}	C=C torsion	224	278	250	43 C=C τ, 29 NH_2 τ, 82 NH_2 wa
ν_{24}	CC_2 wag	184	188	173	51 CC_2 wa, 22 CC≡N sδ, 28 C=C τ

[a] Approximate assignment taking into account also comparison of the spectra of all three samples.
[b] Observed frequencies are from liquid if are available.
[c] Calculated using scaling factors mentioned in text.
[d] Potential energy distribution for scaled frequencies.

Table VIII. Comparison of Observed and Calculated Vibrational Frequencies for *anti* MAM.

No.	Fundamental[a]	Obs.[b]	ab Initio	Scaled[c]	PED[d]
ν_1 A'	N—H stretch	3330	3809	3308	99 NH s
ν_2	=C—H stretch	3090	3366	3079	99 CH s
ν_3	CH_3 asym stretch	3036	3301	3020	98 CH_3 as
ν_4	CH_3 sym stretch	2974	3196	2924	98 CH_3 ss
ν_5	C≡N stretch	2215	2588	2215	86 C≡N s
ν_6	C≡N stretch	2205	2579	2208	86 C≡N s
ν_7	C=C stretch	1648	1829	1676	32 C=C s, 34 CH ro, 24 NH ro
ν_8	N—H rock	1485	1637	1492	16 NH ro, 42 CH_3 aδ, 19 C=C s
ν_9	CH_3 asym bend	1460	1612	1467	36 CH_3 aδ, 36 CH_3 sδ, 21 NH ro
ν_{10}	CH_3 sym bend	1426	1577	1438	57 CH_3 sδ, 15 CH_3 aδ, 16 C=C s
ν_{11}	=C—H rock	1360	1489	1360	23 CH ro, 19 NH ro, 14 C—N s
ν_{12}	=C—N stretch	1337	1444	1319	45 C—N s, 20 CH ro
ν_{13}	CC_2 asym stretch	1231	1341	1224	39 CC_2 as, 13 N—CH_3 s
ν_{14}	CH_3 sym rock	1123	1236	1128	42 CH_3 ro, 18 N—CH_3 s, 17 CC_2 as
ν_{15}	N—CH_3 stretch	992	1097	1007	47 N—CH_3 s, 22 CH_3 ro, 11 CH ro
ν_{16}	CC_2 sym stretch	808	880	801	32 CC_2 ss, 13 CC_2 δ, 12 C=CN δ
ν_{17}	CC_2 deformation	602	659	594	24 CC_2 δ, 25 CC≡N sδ, 28 CC_2 as
ν_{18}	C—C≡N asym bend	526	582	524	27 CC≡N aδ, 26 CC_2 ro
ν_{19}	C=C—N bend	436	484	439	15 C=CN δ, 28 CNC δ, 12 CC≡N aδ
ν_{20}	C—N—C bend	338	364	327	41 CNC δ, 21 C=CN δ, 35 CC≡N aδ
ν_{21}	C—C≡N sym bend	161	153	137	58 CC≡N sδ, 55 CC_2 δ
ν_{22}	CC_2 rock	107	125	113	46 CC_2 ro, 23 CC≡N aδ, 25 C=CN δ
ν_{23} A"	CH_3 asym stretch	2974	3271	2992	100 CH_3 as
ν_{24}	CH_3 asym bend	1443	1589	1445	93 CH_3 aδ
ν_{25}	CH_3 asym rock	1136	1245	1133	90 CH_3 ro
ν_{26}	=C—H wag	992	1123	989	79 CH wa
ν_{27}	N—H wag	710	740	668	12 NH wa, 20 C—N τ, 24 CC≡N sδ
ν_{28}	C—C≡N sym bend	579	649	578	34 CC≡N sδ, 11 CC_2 wa, 22 NH wa
ν_{29}	C—C≡N asym bend	482	546	482	77 CC≡N aδ, 8 C=C τ
ν_{30}	C=C torsion	330	335	304	31 C=C τ, 17 CC≡N aδ, 19 CC≡N sδ
ν_{31}	CC_2 wag	213	185	170	39 CC_2 wa, 14 CC≡N sδ, 47 C=C τ
ν_{32}	=C—N torsion	123	129	118	34 C—N τ, 14 NH wa, 14 CC_2 wa
ν_{33}	CH_3 torsion	76	49	45	46[e] CH_3 τ, 28 NH wa, 8 C—N τ

[a] Approximate assignment taking into account also comparison of the spectra of all three samples.
[b] Observed frequencies are from liquid if are available.
[c] Calculated using scaling factors mentioned in text.
[d] Potential energy distribution for scaled frequencies.
[e] Relative values.

Interaction of the nitrogen lone electron pair with the π-electron system of the carbon-carbon double bond results in decreasing the multiple character of this bond and increasing the carbon-nitrogen bond order. These facts can be documented by a comparison of the carbon-carbon double bond length in ethylene 1.332 Å [32], vinylamine 1.335 Å [26], acrylonitrile 1.343 Å [33], and the present enamines 1.357-1.367 Å. The length of the C—N bond is shortened from the values 1.474-1.465 Å for methylamine [25, 34, 35] over values 1.431 and 1.397 Å for phenyl- and vinylamine [36, 26] and the value 1.352 Å for formamide [37] to the calculated values 1.323-1.327 Å for the enamines.

The calculated C=C and C—N bond lengths for our enamines indicate a highly conjugated system, and the calculated planar or nearly planar structure for all three samples is not surprising. The tendency of forming a planar structure with a higher degree of conjugation appears from the angle between the NH_2 plane and the extension of the C—N bond. This angle is 54.3° for methylamine, 38° and 34° for phenyl- and vinylamine, and nearly zero for the nearly planar structures of gaseous or solid formamide, acetamide, and *N*-methylacetamide [38-40].

A more detailed ab initio geometry discussion with charge distributions for these enamines and for other similar compounds will appear shortly [41, 42].

Conformational Energy

The conformational energies of MAM calculated by the ab initio and semiempirical methods are approx-

Table IX. Comparison of Observed and Calculated Vibrational Frequencies for *syn* MAM.

No.	Fundamentals[a]	Obs.[b]	ab Initio	Scaled[c]	PED[d]
ν_1 A'	N—H stretch		3874	3364	99 NH s
ν_2	=C—H stretch		3364	3077	99 CH s
ν_3	CH_3 asym stretch		3298	3017	99 CH_3 as
ν_4	CH_3 sym stretch		3210	2937	99 CH_3 ss
ν_5	C≡N stretch		2591	2216	89 C≡N s
ν_6	C≡N stretch		2584	2213	87 C≡N s
ν_7	C=C stretch	1629	1785	1638	54 C=C s, 30 C—N s, 27 CH ro
ν_8	N—H rock	1548	1705	1555	69 NH ro, 21 C—N s
ν_9	CH_3 asym bend		1614	1467	90 CH_3 aδ
ν_{10}	CH_3 sym bend		1580	1437	99 CH_3 sδ
ν_{11}	=C—N stretch	1369	1501	1370	56 CH ro, 21 C=C s
ν_{12}	=C—H rock	1305	1416	1297	27 C—N s, 22 NH ro, 15 N—CH_3 s
ν_{13}	CC_2 asym stretch	1209	1333	1215	31 CC_2 as, 25 CH_3 ro
ν_{14}	CH_3 sym rock		1255	1143	41 CH_3 ro, 28 CC_2 as
ν_{15}	N—CH_3 stretch		1043	959	65 N—CH_3 s, 11 C—N s
ν_{16}	CC_2 sym stretch	782	857	781	17 CC_2 ss, 11 CC_2 as, 34 C=CN δ
ν_{17}	CC_2 deformation		676	608	29 CC_2 δ, 29 CC≡N sδ, 23 CC_2 ss
ν_{18}	C=C—N bend	571	654	597	10 C=CN δ, 17 CNC δ, 26 CC_2 ss
ν_{19}	C—C≡N asym bend	452	511	455	58 CC≡N aδ, 15 CC_2 ro, 11 C=CN δ
ν_{20}	C—N—C bend	263	282	256	57 CNC δ, 21 C=CN δ, 17 CC_2 ro
ν_{21}	CC_2 rock		171	154	46 CC_2 ro, 25 CC≡N aδ, 16 C=CN δ
ν_{22}	C—C≡N sym bend		163	145	64 CC≡N sδ, 59 CC_2 δ
ν_{23} A''	CH_3 asym stretch		3309	3027	100 CH_3 as
ν_{24}	CH_3 asym bend		1595	1450	92 CH_3 aδ
ν_{25}	CH_3 asym rock		1241	1129	86 CH_3 ro
ν_{26}	=C—H wag		1113	978	80 CH wa
ν_{27}	C—C≡N sym bend	689	713	645	45 CC≡N sδ, 30 CC_2 wa, 10 C—N τ
ν_{28}	C—C≡N asym bend	490	566	506	33 CC≡N aδ, 9 C=C τ, 16 C—N τ
ν_{29}	N—H wag		502	449	19 NH wa, 42 C—N τ, 41 CC≡N aδ
ν_{30}	C=C torsion		392	346	26 C=C τ, 17 CC≡N aδ, 60 NH wa
ν_{31}	CC_2 wag		203	186	65 CC_2 wa, 31 CC≡N sδ
ν_{32}	CH_3 torsion		153	143	80[e] CH_3 τ
ν_{33}	=C—N torsion		76	70	32[e] C—N τ, 39 C=C τ, 12 NH wa

[a] Approximate assignment taking into account also comparison of the spectra of all three samples.
[b] Observed frequencies are from liquid if are available.
[c] Calculated using scaling factors mentioned in text.
[d] Potential energy distribution for scaled frequencies.
[e] Relative values.

imately two to three times higher than the experimental values determined from IR and NMR spectra. The best results have been achieved with ab initio at the MP2/SCF level and with AM1 methods. The difference between experimental and calculated values may be attributed to possible interactions of the highly polar MAM molecule with the polar solvents (acetonitrile and DMSO) used for the experimental energy determination compared with the isolated molecule in the calculations.

NMR Spectra

All the spectra contain characteristic shifts in the region expected for nitrile carbon atoms (114–118 ppm). Owing to the two nitrile substituents, the adjacent olefinic carbon atoms are extremely high field shifted (45–48 ppm) in contrast to the other olefinic carbons with a corresponding low field shift (158–162 ppm). Depending on the stereochemical effects, the methyl groups absorb in the region 30 to 47 ppm. In the spectrum of MAM, two different subspectra appear, to be assiend to *anti* and *syn* conformers. It is known from other methylated amino compounds with partial double bonds between nitrogen and the neighboring atom (dimethylformamide, dimethylacetamide, etc.) that restriction of the rotational motion results in different chemical shifts of the methyl groups. Thus, two chemical CH_3 shifts for DMAM have been observed.

Table X. Comparison of Observed and Calculated Vibrational Frequencies for DMAM.

No.	Fundamental[a]	Obs.[b]	ab Initio	Scaled[c]	PED[d]
ν_1	=C−H stretch	3081	3370	3083	98 CH s
ν_2	CH_3 asym stretch	3030	3316	3033	95 CH_3 as
ν_3	CH_3 asym stretch	3030	3306	3024	89 CH_3 as
ν_4	CH_3 asym stretch	3011	3296	3015	94 CH_3 as
ν_5	CH_3 asym stretch	2980	3259	2981	99 CH_3 as
ν_6	CH_3 sym stretch	2930	3209	2936	94 CH_3 ss
ν_7	CH_3 sym stretch	2924	3187	2916	93 CH_3 ss
ν_8	C≡N stretch	2217	2588	2213	88 C≡N s
ν_9	C≡N stretch	2205	2580	2209	88 C≡N s
ν_{10}	C=C stretch	1638	1789	1641	42 C=C s, 40 C−N s, 26 C−H ro
ν_{11}	CH_3 asym bend	1482	1635	1489	55 CH_3 aδ, 15 CH_3 ro
ν_{12}	CH_3 asym bend	1482	1617	1471	72 CH_3 aδ, 11 CH_3 ro
ν_{13}	CH_3 asym bend	1449	1604	1458	83 CH_3 aδ
ν_{14}	CH_3 sym bend	1436	1593	1449	76 CH_3 sδ
ν_{15}	CH_3 asym bend	1436	1590	1446	84 CH_3 aδ
ν_{16}	CH_3 sym bend	1424	1573	1430	105 CH_3 sδ
ν_{17}	=C−N stretch	1408	1556	1423	26 C−N s, 14 NC_2 as, 24 CH_3 aδ
ν_{18}	=C−H rock	1368	1511	1381	47 C−H ro, 26 C=C s
ν_{19}	NC_2 asym stretch	1264	1417	1296	38 NC_2 as, 11 CC_2 as, 17 CH_3 ro
ν_{20}	CC_2 asym stretch	1172	1272	1161	50 CC_2 as, 11 NC_2 as, 14 CC_2 ro
ν_{21}	CH_3 asym rock	1154	1259	1145	87 CH_3 ro
ν_{22}	CH_3 sym rock	1129	1231	1123	56 CH_3 ro
ν_{23}	CH_3 asym rock	1100	1216	1105	84 CH_3 ro
ν_{24}	CH_3 sym rock	1059	1171	1070	61 CH_3 ro
ν_{25}	=C−H wag	954	1106	971	81 C−H wa
ν_{26}	NC_2 sym stretch	859	936	860	68 NC_2 ss, 10 CC_2 ss
ν_{27}	CC_2 sym stretch	817	882	804	19 CC_2 ss, 29 C=CN δ, 10 CC_2 as
ν_{28}	C−C≡N sym bend	625	706	637	51 CC≡N sδ, 37 CC_2 wa
ν_{29}	CC_2 deformation	585	679	611	28 CC_2 δ, 38 CC≡N sδ, 26 CC_2 ss
ν_{30}	C−C≡N asym bend	548	602	547	16 CC≡N aδ, 15 CC_2 ro, 17 NC_2 δ
ν_{31}	C−C≡N asym bend	498	558	496	59 CC≡N aδ, 13 C=C τ
ν_{32}	C=C−N bend	444	497	445	15 C=CN δ, 20 NC_2 ro, 15 CC≡N sδ
ν_{33}	NC_2 deformation	400	442	402	43 NC_2 δ
ν_{34}	C=C torsion	391	432	392	10 C=C τ, 28 CC≡N aδ, 18 NC_2 δ
ν_{35}	NC_2 rock	289	300	272	43 NC_2 ro, 24 C=CN δ, 18 CC≡N aδ
ν_{36}	NC_2 wag	261	271	252	30 NC_2 wa, 19 CC_2 wa, 15 CC≡N sδ
ν_{37}	CC_2 wag	176	180	166	33 CC_2 wa, 13 CC≡N sδ, 61 CH_3 τ
ν_{38}	CC_2 rock	168	169	153	22 CC_2 ro, 17 CC≡N aδ, 18 CC≡N sδ
ν_{39}	C−C≡N sym bend	158	154	139	58 CC≡N sδ, 41 CC_2 δ
ν_{40}	CH_3 torsion	100	144	132	37 CH_3 τ, 18 CC_2 ro, 12 CC≡N aδ
ν_{41}	CH_3 torsion	92	99	92	42[e] CH_3 τ, 46 NC_2 wa
ν_{42}	=C−N torsion	58	31	29	27[e] C−N τ, 43 CH_3 τ, 13 C=C τ

[a] Approximate description taking into account also comparison of the spectra of all three samples.
[b] Observed frequencies are from the solution if are available.
[c] Calculated using scaling factors mentioned in text.
[d] Potential energy distribution for scaled frequencies.
[e] Relative values.

Evidence of the conformers and a total assignment of the spectra are given by evaluating the vicinal coupling constants $^3J_{HC}$ derived from proton-coupled ^{13}C NMR spectra. C_7 and C_9 can be easily assigned by comparing the coupling to H_5. The *trans* coupling (dihedral angle 180°) exceeds the *cis* coupling (0°) approximately by a factor of 2.

Similar behavior of the vicinal coupling constants between C_4 and C_6 with H_5 establishes the assignment of the corresponding chemical shifts. Comparing these values for DMAM (6.5 Hz *trans* coupling; 5.1 Hz *cis* coupling) and the corresponding coupling constants for the methyl groups of the MAM conformer mixture (5.3 Hz for *anti* and 7.9 Hz for *syn*), the assignment of Table

IV was obtained. Additional evidence for the two conformers is derived from the predominant *anti* conformer (ratio *anti*:*syn* is ca. 4:1, leading to the value of ca. 3.5 kJ mol^{-1} for Gibbs free energy at room temperature).

The substitution of one amine proton of AM forming the *anti* conformer of MAM does not change significantly the chemical shift of C_7 and C_9. On the other hand, the same substitution in the *syn* position results in a downfield shift of 1.5 ppm at C_9, leaving the chemical shift of C_7 unchanged. Substitution of the other proton by a methyl group in DMAM has no further influence. This fact suggests that steric interaction exists between the *syn*-methyl and nitrile in position 9. As a result, the R_1-N-R_2 plane seems to be twisted slightly against the plane of the olefinic part of DMAM and probable *syn* in MAM, too. Twisting around the C_2-N_3 axis changes the dihedral angles H_5-C_2-N_3-C_4 and H_5-C_2-N_3-C_6, reducing both the *trans* and *cis* coupling constants according to the Karplus curve. The numerical values of Table IV reflect this tendency. Vicinal coupling constant H_4-C_1 is also reduced, introducing a methyl group in position 6. Finally, introducing the second methyl group in the *anti* or *syn* conformers of MAM results in considerably different beta effects for the existing methyl carbons, caused predominantly by steric interaction. This is an additional indication for twisting mentioned above.

Vibrational Spectra

Since the N—H stretching modes give rise to the bands with the highest wave numbers, their assignment in the vibrational spectra for AM and MAM is straightforward. A doublet band structure was observed for these vibrational modes in the solid and solution spectra. The splitting can be attributed to enamine association or in solution interaction with the solvent molecules. These interactions are stronger in the solid phase where N—H frequencies are lower than in solutions. The association process is typical for amines, and the higher frequency corresponds to vibration of the free N—H bond, the lower frequency to vibration of the associated N—H bond.

The band with the highest wave numbers in the C—H frequency region has been assigned as the =C—H stretching mode. Such an assignment corresponds to the frequencies of the C—H bonds for trisubstituted ethylene. The assignment of the CH_3 stretching modes is not clear without additional isotopic studies and is based only on the normal coordinate calculations.

The C≡N stretching modes were found between 2200 and 2220 cm^{-1}, and they are in the expected region [43]. According to PED, the higher-frequency band corresponds to C≡N stretch in the *trans* position to the amino group.

The frequency shifts of the C=C stretching mode (1662 cm^{-1} for AM, 1648 and 1630 cm^{-1} for *anti* and *syn* conformers of MAM, and 1644 cm^{-1} for DMAM) can be explained by the inductive effect of the *N*-methyl groups as was done for *N*-methyl derivatives of formamide and acetamide [40]. The shifts measured here are about half of those for *N*-methyl derivatives of formamide and acetamide and confirm the calculated slight decrease of the double-bond character of the C=C bond and the increase of the double-bond character of C—N bond from AM to DMAM. These conclusions are also supported by the increasing frequencies of the C—N stretching modes from 1329 cm^{-1} for AM to 1408 cm^{-1} for DMAM.

The vibrational frequencies of amino deformation modes—1591 cm^{-1} for NH_2 scissoring and 1485 cm^{-1} for NH rocking—are slightly below the region of such vibrations for nonplanar amines. However, these frequencies are in the expected region in planar or practically planar amides. The last in-plane vibrational mode of the amino group—NH_2 rocking—was assigned according to the normal coordinate calculation at 1099 cm^{-1}. This value is in the region for the NH_2 twisting mode of amines and NH_2 rocking mode for amides.

The bands at 623 cm^{-1} and 298 cm^{-1} were assigned as the nonplanar vibrational modes of the NH_2 group. The first band corresponds to the NH_2 torsional mode, the second to the NH_2 wagging mode. The band at 710 cm^{-1} was assigned to NH wagging mode. According to the calculated PED, the bands at 567 cm^{-1} for AM and 579 cm^{-1} for MAM could also be assigned to such modes. However, common features of both the 623-cm^{-1} and 710-cm^{-1} bands—strong and broad bands in IR spectra and absence in Raman spectra—and the fact that a band of such character is not present in this region in the vibrational spectra of DMAM indicate the assignment of the 623-cm^{-1} and 710-cm^{-1} bands to amino groups. Also, a higher frequency for the NH_2 torsional mode compared with the NH_2 wagging mode is characteristic for planar amides rather than for nonplanar aliphatic or aromatic amines where the NH_2 wagging mode is in the region 700–850 cm^{-1} [43]. This means that the measured lower frequency of 623 cm^{-1} for the NH_2 out-of-plane mode supports the planar structure of the amino group.

According to PED, the vibrational frequencies of the =C—H rocking and wagging modes have been as-

signed in the narrow intervals 1350–1368 cm^{-1} and 954–1002 cm^{-1}, respectively, in the regions expected for trisubstituted ethylene.

Eight bending modes are associated with the $=C(CN)_2$ group, and their assignment is not straightforward like for other compounds with a $C(CN)_2$ group, e.g., 1,1-dicyanocyclopropane [30], 1,1-dicyanocyclobutane [31], carbonyl cyanide [44], and propanedinitrile [45]. The calculations indicate that each of the four C—C≡N linear bending modes is mixed with one of the four deformation modes of the $=CC_2$ group. The CC_2 scissor is mixed with the in-plane symmetric linear bending mode of both CC≡N groups, and the CC_2 rock is mixed with the in-plane CC≡N asymmetric linear bending mode. The CC_2 wag is mixed with the out-of-plane symmetric linear bending mode of both CC≡N groups. The CC_2 twist for a nonplanar $>CC_2$ structure or the C=C torsional mode for a planar $=CC_2$ structure is mixed with the out-of-plane asymmetric CC≡N linear bending mode. In each mentioned pair one mode should occur between 400 and 600 cm^{-1} and the other between 100 and 300 cm^{-1}.

The out-of-plane asymmetric CC≡N linear bending appears as the most localized mode according to the PED, and therefore its assignment is the most straightforward among the bands in the narrow region 475–498 cm^{-1} for all three samples. This mode has also been found for 1,1-dicyanocyclopropane and for 1,1-dicyanocyclobutane [30, 31] in this region. On the other hand, the corresponding C=C torsional mode interacts with other fundamentals and suffers the largest frequency shift from 224 cm^{-1} for AM to 391 cm^{-1} for DMAM.

The CC_2 scissoring and the in-plane symmetric CC≡N linear bending modes are both highly mixed as previously reported for 1,1-dicyanocyclopropane and 1,1-dicyanocyclobutane [30, 31]. The assignment of these two modes is not straightforward by normal coordinates calculations, and from the results for related compounds [30, 31, 44], we assigned the CC_2 scissoring mode in the high-frequency region 585–605 cm^{-1} and the corresponding CC≡N linear bend in the low-frequency range.

The two remaining CC_2 modes (rocking and wagging), although mixed with the mentioned CC≡N modes, should occur in the low-frequency region. The CC≡N bending modes have been assigned in the regions 526–552 cm^{-1} (the in-plane asymmetric linear bend) and 567–625 cm^{-1} (the out-of-plane symmetric linear bend), respectively. The C=C—N bending mode was assigned for all three samples to a band with very similar character in the narrow frequency interval 424–444 cm^{-1}.

The assignment of the deformation modes and especially of the torsional modes below 250 cm^{-1} is very tentative because spectral data from the fluid phases are missing in this region and many lattice modes for AM and MAM are present in the solid-phase spectra.

ACKNOWLEDGMENTS

The authors are grateful to Professor R. Salzer and to G. Woelki from the TU Dresden and to A. Horn from the University of Oslo for help with the experimtnal work and to a referee who suggested important improvements. A.G. gratefully acknowledges "die Konferenz der deutschen Akademien der Wissenschaften" for a scholarship.

REFERENCES

1. Cook, A. G., Ed., *Enamines: Synthesis, Structure and Reactions*; Marcel Dekker: New York, 1969.
2. Dyke, S. F. *The Chemistry of Enamines*; Cambridge University Press: London, 1973.
3. Albrecht, R. *Prog. Res.* **1977,** *21,* 9.
4. Bouzard, D. In *Recent Progress in the Chemical Synthesis of Antibiotics*; Springer-Verlag: München, 1990; p. 249.
5. Freeman, F. In LONZA *Reaction of Malononitrile Derivatives*; Georg Thieme Verlag: Stuttgart, 1981; *Synthesis* **1981,** p. 925.
6. F. Hoffmann-La Roche & Co., *Netherland Appl.* 6613489 **1967;** *C. A.* **1967,** *67,* 52727g.
7. Nomura, H.; Sugimoto, K.; Shirai, M. Japanese Patent 14204 **1968;** *C. A.* **1969,** *71,* 12607g.
8. Tadashi, F.; Katsuaki, H. Japanese Patent 25570 **1969;** *C. A.* **1970,** *72,* 12165g.
9. Kondo, O.; Takada, M.; Matsumoto, N. Japanese Patent 2414 **1965;** *C. A.* **1965,** *62,* 14508f.
10. Leimgruber, W.; Weigele, M. U.S. Patent 3542848 **1970;** *C. A.* **1971,** *74,* 41945h.
11. Shvo, Y.; Taylor, E. C.; Bartulin, J. *Tetrahedron Lett.* **1967,** [illegible], 3259.
12. Shvo, Y.; Shavan-Atidi, H. *J. Am. Chem. Soc.* **1969,** *91,* 6683, 6689.
13. Hobson, R. F.; Reeves, L. W. *J. Phys. Chem.* **1973,** *77,* 419.
14. Scheibe, P.; Schneider, S.; Doerr, S.; Daltrozzo, E. *Ber. Bunsegges. Phys. Chem.* **1976,** *80,* 630.
15. Uray, G.; Wolfbeis, O. S.; Junek, H. *J. Mol. Struct.* **1979,** *54,* 77.
16. Krasnaya, Zh. A.; Bogdanov, V. S. *Izv. Akad. Nauk SSR, Ser. Khim.* **1991,** 2348.
17. Didkovskii, V. E.; Egorov, Yu. P.; Baranskii, V. A.; Yatsizhin, A. A.; Pavlenko, N. G.; Kukhar, V. P. *Dopov. Akad. Nauk Ukr. RSR, Ser. B: Geol., Khim Biol. Nauki* **1980,** 40.
18. Diels, O.; Gärtner, H.; Kaack, R. *Ber. Dtsch. Chem. Ges. B* **1922,** *55,* 3439.
19. Eiden, P. *Angew. Chem.* **1960,** *72,* 77.: Meerwein, H.; Werner, F.; Schön, N.; Stopp, G. *Justus Liebig Ann. Chem.* **1961,** *641,* 1-39.

20. Trofimenko, S. *J. Org. Chem.* **1963,** *28,* 2755.
21. Liptaj, T.; Pronayova, N., to be published.
22. Stewart, J. J. P. *QCPE Bull.* **1983,** *3,* 101.
23. Huzinaga, S. *J. Chem. Phys.* **1965,** *42,* 1293.
24. Dunning, T. H. *J. Chem. Phys.* **1970,** *53,* 2823.
25. Takagi, K.; Kojima, T. *J. Phys. Soc. Jpn.* **1971,** *30,* 1145.
26. Lovas, F. J.; Clark, F. O.; Tiemann, E. *J. Chem. Phys.* **1975,** *62,* 1925.
27. Adams, D. B. *J. Chem. Soc., Perkin Trans.* **1993,** *2,* 567.
28. Durig, J. R. In *13th Int. Conf. on Raman Spectroscop*; Kiefer, W.; Cardona, M.; Schaach, G.; Schneider, F. W.; Schrötter, H. W., Eds.; Wiley: Chichester, 1992; p 44.
29. Pulay, P.; Fogarasi, G.; Pongor, G.; Boggs, J. E.; Vargha, A. *J. Am. Chem. Soc.* **1983,** *105,* 7037.
30. Little, T. S.; Zhao, W.; Durig, J. R. *J. Raman Spectrosoc.* **1988,** *19,* 479.
31. Durig, J. R.; Zhao, W.; Little, T. S.; Dakkouri, M. *Chem. Phys.* **1988,** *128,* 335.
32. Bartell, L. S.; Bonham, R. A. *J. Chem. Phys.* **1959,** *31,* 400.
33. Fukuyama, T.; Kuchitsu, K. *J. Mol. Struct.* **1970,** *5,* 131.
34. Lide, D. F. *J. Chem. Phys.* **1957,** *27,* 343.
35. Higginbotham, H. K.; Bartell, L. S. *J. Chem. Phys.* **1965,** *42,* 1131.
36. Hatta, A.; Suzuki, M.; Kozima, K. *Bull. Chem. Soc. Japan,* **1973,** *46,* 2321.
37. Hirota, E.; Sugisaki, R.; Nielsen, C. J.; Sorensen, G. O. *J. Mol. Spectrosc.* **1974,** *49,* 251.
38. Costain, C. C.; Dowling, J. M.; *J. Chem. Phys.* **1960,** *32,* 158.
39. King, S. T. *Spectrochim. Acta* **1972,** *28A,* 165.
40. Popov, E. M.; Zheltova, V. N. *J. Mol. Struct.* **1971,** *10,* 221.
41. Sklenák, Š.; Biskupič, S.; Gatial, A. *J. Chem. Soc.* (submitted).
42. Sklenák, Š.; Biskupič, S.; Gatial, A. *Models in Chemistry* (submitted).
43. Roeges, N. P. G. *A Guide to the Complete Interpretation of Infrared Spectra of Organic Structures*; Wiley: Chichester, 1994.
44. Miller, F. A.; Harney, B. M. *Spectrochim. Acta* **1971,** *27A,* 1003.
45. Fujiyama, T.; Shimanouchi, T. *Spectrochim. Acta* **1964,** *20,* 829.